Coherent Soft X-ray Diffraction Imaging of Coliphage PR772 at the Linac Coherent Light Source

Authors

First Authors:
Hemanth K. N. Reddy, Kartik Ayyer
Corresponding Authors: Johan Bielecki, Andrew Aquila

Affiliations

Abstract (170w)

Single-particle diffraction from X-ray Free Electron Lasers offers the potential for molecular structure determination without the need for crystallization. In an effort to further develop the technique, we present a dataset of coherent soft X-ray diffraction images of Coliphage PR772 virus, collected at the Atomic Molecular Optics (AMO) beamline with pnCCD detectors in the LAMP instrument at the Linac Coherent Light Source. The diameter of PR772 ranges from 65 - 70 nm, which is considerably smaller than the previously reported ~600 nm diameter Mimivirus. This reflects continued progress in XFEL-based single-particle imaging towards the single molecular imaging regime. The data set contains significantly more single particle hits than collected in previous experiments, enabling the development of improved statistical analysis, reconstruction algorithms, and quantitative metrics to determine resolution and self-consistency.

Background & Summary Abstract (700w)

Theoretical studies predict X-ray Free Electron Lasers (XFELs) can potentially image biomolecules and hence determine their structures without crystallization [Neutze 2000]. To realize this in practice has proved a significant experimental challenge. The Single Particle Imaging (SPI) Initiative [Aquila 2015] was formed as a collaborative effort to identify and solve the experimental challenges to achieving high-resolution imaging of single molecules with X-rays.

Coliphage PR772 is a virus of approximately 70 nm in diameter, which infects *Escherichia coli* (*E. coli*). It was selected as the sample for this experiment due to its high structural homogeneity, uniform size distribution, suitable particle concentration in solution, having a known structure, and the ability to be aerosolized by Gas Dynamic Virtual Nozzle (GDVN) [DePonte 2008] for injection into the XFEL beam using an aerosol injector. Having a known structure of PR772 (unpublished) enables validation of any subsequent data analysis steps.

For the data presented here, Coliphage PR772 was aerosolized and delivered into the focus of the LAMP instrument at the Atomic Molecular Optics (AMO) beamline [Ferguson 2015] of the Linac Coherent Light Source (LCLS) X-ray laser [Emma 2010 & White 2015]. The data include clear diffraction snapshots from single PR772 virus particles.

SLAC National Accelerator Laboratory, 2575 Sand Hill Road, Menlo Park, CA 94025

This material is based upon work supported by the U.S. Department of Energy, Office of Science, under Contract No. DE-AC02-76SF00515.

Methods

Sample Preparation

Bacteriophage PR772 (ATCC BAA-769-B1) infects *E.coli* K12 J53-1 (ATCC BAA-769). PR772 was cultured on agar by the overlay method. Tryptic Soy Agar (Difco™ Tryptic Soy Agar) was prepared and poured into petri dishes to form a hard agar support layer. The overlay medium was soft agar prepared with Tryptic Soy Broth (Bacto™ Tryptic Soy Broth) along with 0.5% Agar-Agar (Microbiology, Merck). *E. coli* was cultured in Tryptic Soy Broth to reach an OD_{600} of 0.7. Soft agar was melted and cooled to 45°C. *E. coli* and viral stock (10^8 pfu/mL) were added to the soft agar in a volume ratio of 10:1 and mixed well. The mixture was immediately poured onto the hard agar in the petri dishes and incubated overnight at 37°C.

The soft agar layer from the overnight culture was scraped off and collected in a sterile container, diluted with 100 mL of sterile storage buffer (TRIS 50mM, NaCl 100mM, $MgSO_4$ 1mM, EDTA 1mM, pH 8.0) and mixed overnight at 4°C. The mixture was centrifuged at 8000 g for 30 min to remove agar and cell debris. The supernatant was collected and filtered through a 0.45 micron filter (Filtropur S 0.45, Sarstedt). The viral particles were separated from the permeate solution by PEG precipitation (9% w/v PEG 8000 and 5.8% w/v NaCl). After mixing overnight at 4°C, the precipitate was centrifuged for 90 min at 8000 g. The supernatant was discarded and the viral pellet was suspended in 1 mL storage buffer. The viral suspension was then applied to a Capto-Q anion exchange column. The sample was eluted by varying the concentration of NaCl (100 mM – 1.5 M). The fractions representing the elution profile peak was collected and observed with a electron microscopy (EM) (Quanta FEG 650, FEI) to confirm the presence of intact viral particles. (Figure 1)

Before sample injection, the PR772 was transferred from storage buffer into volatile ammonium acetate buffer (250mM, pH 7.5) using PD10 desalting columns (GE Healthcare). Hence, most assays were performed with sample in ammonium acetate buffer instead of storage buffer.

Sample Characterization

Infectivity

Virus titers were measured by plaque assay following purification purification [Mazzocco 2009]. Serial 10-fold dilutions of purified virus were plated on a mat of *E. coli* and incubated overnight at 37 degrees C. Plaque forming units per mL (pfu/mL) were calculated using the formula: average # plaques/volume plated x dilution.

Liquid Phase

The size and monodispersity of the PR772 in ammonium acetate buffer were measured using Nanoparticle Tracking Analysis (NTA) (NanoSight LM10, Malvern Instruments Ltd.) (Figure 2) and Dynamic Light Scattering (DLS) (w130i, AvidNano Ltd.) (Figure 2). The sample was diluted to the required concentrations for measurement. For NTA 10^8 particles/mL were used to limit the number of tracks to 200. For DLS about 10^{10} particles/mL was used to reach a recommended counts/s.

Gaseous Phase

The size distribution in the gas phase was measured using Electrophoretic DMA (Figure 2). PR772 was aerosolized with a nano-electrospray ionization (ESI) source (TSI model 3480) and passed through an electrostatic classifier (TSI model 3480) to continuously classify particles from 10 nm to 500 nm. Classified particles were counted with a condensation particle counter (CPC, TSI model 3786).

Injection Testing

Injection tests on PR772 were performed with a setup similar to the one subsequently used at the LCLS experiment to investigate the aerosolization characteristics of the samples and to study sample behavior during the injection procedure [Hantke 2014]. A glass microscope slide covered by a transparent sticky gel piece (GelPak) was positioned beneath the exit point of the aerodynamic lens (at a position similar to the interaction region with the X-ray beam at LCLS). Particle dusting spots were observed through an objective lens mounted below the glass slide. The focused particles from the injector were also collected on formvar/carbon grids (#01754F, F/C 400 mesh Cu, Ted Pella Inc.). These samples were examined by EM without any further modification.

Sample Injection at LCLS

Samples were delivered into the X-ray beam using the aerodynamic lens stack system used in previous experiments. [Munke 2016] Purified PR772 was transferred to a volatile ammonium acetate buffer at a concentration of 10^{12} particles mL^{-1} and introduced to the injector via a GDVN [DePonte 2008] at a flow rate of 1-2 µL min^{-1}. The aerosol continued through a gas skimmer and a relaxation chamber, forming a fine beam of focused particles by the aerodynamic lens stack [Bogan 2008]. The focus of the particle beam and multiplicity of the particles could be optimized by regulating the flow of sample and gas along with the skimmer pressure.

Experimental Setup and Data Collection

Coherent diffraction snapshots using single soft X-ray pulses were recorded at the AMO beamline of the LCLS XFEL using the LAMP endstation [Ferguson 2015]. The configuration was similar to that used in previous coherent diffraction experiments [Seibert 2010], but with a shorter distance from the sample interaction region to the detector due to the gate valve between detector and sample chambers being removed for the present experiment.

Measurements were performed using LCLS tuned to a photon energy of 1.6 keV delivering 4 mJ into a 70 fs duration pulse at the end of the undulators. This was focused into a nominal 1.5 μm^2 FWHM region using a pair of Kirkpatrick-Baez (KB) mirrors, giving a nominal power density of ~3.8 10^{18} W/cm^2 or 10^{13} photons per pulse assuming no beamline losses. Comparison of measured and calculated from known scattering objects indicate that the actual power density may differ from this estimate by a factor of 10. This is due to three combined effect of overfilling of the focusing optics, carbon contamination on the KB mirrors increasing mirror roughness (reducing reflectivity), and a less-than-perfect focal spot size due to carbon contamination distorting the KB mirrors (increasing effective focal spot size).

The photon energy was selected by considering the highest achievable resolution, while remaining below the silicon absorption edge at 1.8 keV. At photon energies above the silicon K-edge of 1.8 keV, the silicon beam conditioning apertures' fluorescence increases the background. A series of silicon apertures, including a post-sample aperture, were used to limit the amount of background scatter incident on the detectors from the beamline. Three 1mm x 1mm Si_3N_4 apertures were used to reduce low q scatter. The first two apertures were positioned laterally to the beam to form a small rectangle, with the third aperture used to clean up diffraction from the first two. The first two apertures were separated by 5 cm, with the third aperture separated by 10 cm. Additionally the third aperture was 10 cm away from the focus. A large round aluminum post sample aperture was used to block high q scatter. It was located 2.4 cm downstream of the sample with a diameter of 4 cm.

Diffraction snapshots were recorded using two pairs of pnCCD detectors [Struder 2010] at the LCLS pulse repetition rate of 120 Hz. One pair of pnCCD detectors was located 10 cm downstream of the interaction region, and a second pair of detectors further downstream at 58.1 cm from the interaction region. The pixel size are 75 µm and each detector in the pair has 512x1024 pixels giving the full set-up a pixel count of two planes each with 1024x1024 pixels. The experimental configuration was similar to that described in [Ekeberg 2015], albeit with a higher photon energy (1.6 keV instead of 1.2 keV) , and the use of a different beam conditioning configuration and the front pnCCD. The majority of the data processing and evaluation of the quality of the data was conducted on the downstream detector. The resolution of the downstream detector is 11.6 nm at the edge or 8.3 nm in the corner giving an oversampling of the diffraction patterns of > 10.

The data were analyzed online using *Hummingbird* [Daurer 2016] and *psana* [Damiani 2016].

Data Processing

Data saved in the native XTC format used at the LCLS were analysed and converted to the CXI file format using the LCLS data analysis framework *psana* [Damiani 2016]. The raw pnCCD pixels contain analog to digital units (ADUs), to which various corrections must be made in order to obtain photon counts. As a first step, dark calibration and row-by-row common mode correction were performed on the pnCCD detector images by the LCLS software environment, *psana*. Data was calibrated using *psana*'s *ImgAlgos.NDArrCalib* module, with pedestal subtraction (*do_peds*), common-mode correction (do_cmod), statistical correction (do_stat) and gain corrections (do_gain) turned on. A flat-field data set using silicon K edge fluorescence (1.7 keV) was used to calibrate the gain on a pixel basis. These gain-corrected ADU values were then thresholded based on an average of 128 ADUs/photon in order to obtain photon counts.
Not all detector frames (or events) contained diffraction from single particles. Since the average number of particles per X-ray focus volume is much less than one, most of the pulses do not hit any particles. Hits (events in which a particle was intercepted by the X-ray beam) were identified using a chi squared metric adapted from [Loh 2012].

$$\chi_j^2 = \frac{\overline{\left(I_j - B_j\right)^2}}{Var\left(B_j\right)}$$

Chi squared for the j[th] image I_j was calculated by subtracting a running median background B and normalizing by the variance of B. The chi squared value was calculated within an annular area of radii 150 and 400 pixels from beam center and hits were defined to frames with Chi-squared above 10. Hits were saved to file with detector corrections applied (i.e., pedestal, common mode and gain corrected) and then down-sampled by a factor of 4.

Single-particle diffraction patterns were identified by analysing all the hits in a reduced set of dimensions using diffusion map embedding similar to the method described in [Yoon 2012] shown in Figure 3. The normalized graph Laplacian is used to calculate the likelihood of diffusion from the center of the single particle cluster at $\Phi_1, \Phi_2, \Phi_3 = -0.75, 0, 0$. A likelihood value of 0.725 or higher is considered inside the single particle cluster. A total of 12,678 out of 14,772 images were identified as single particle hits. An alternative manifold-based data analytical approach yielded a larger dataset consisting of 37,550 single-particle snapshots, whose indices are provided. This approach reveals and corrects intensity variations and a range of other imaging artifacts [A. Hosseinizadeh 2015]. Another method for data sorting and classification is based on principal component analysis (PCA) [Bobkov 2015]. With this approach we have filtered 21,733 images as hits by intensity thresholding (all images above 200k photons). A total of 7,992 images were identified by the PCA technique as single hits and removed outliers by radial intensity filtering (also provided). A comparison of the summation of the single-particle hits, forming a pseudo small angle X-ray scattering patters, is shown in figure 4.

Manual selection was not employed due to the large number of hits and the potential for user bias. Because identification of single-particle hits is dependent on the input parameters for clustering, we have deposited all data frames and identified potential single particle hits as a list of events. This enables the testing and comparison of different hit sorting algorithms.
Raw XTC files are included in the data deposition for anyone wishing to repeat the analysis from scratch.

Data Records

The data are deposited in the Coherent X-ray Imaging Data Bank (CXIDB) [Maia 2012] in the CXIDB data format, which is based on the HDF5 format (Data Citation 1). Convenient functions for accessing the CXIDB data file exist in the libspimage package for C and Python (Maia 2010), as well as many computing environments, including Python using the *h5py* module and MATLAB using e.g. ,the *h5read* function. The Owl software is convenient for visualizing data in the CXIDB format. In addition to the CXI file, the conversion script (create_dataset.py) and additional metadata files (selection.h5, psana.cfg) are provided along with usage instructions. Detector panel calibration files mapping data to real space are also provided. Configuration files for *Hummingbird* and *psana* are provided for completeness of describing processing performed on the deposited data.

Run number	Sample	Number of frames in XTC file	Number of hits
182	PR772	97,733	15
183	PR772	169,227	3
184	PR772	136,624	1
185	PR772	77,079	7

186	PR772	453,285	2,048
188	PR772	322,097	1,171
190	PR772	265,585	1,498
191	PR772	293,284	1,718
192	PR772	224,583	1,279
193	PR772	329,049	2,525
194	PR772	214,891	1,661
196	PR772	204,236	1,436
197	PR772	188,895	1,410
Total		**2,976,568**	**14,772**

Usage Notes

Acknowledgements

Author contributions

Competing interests

The authors declare no competing interests.

Figures

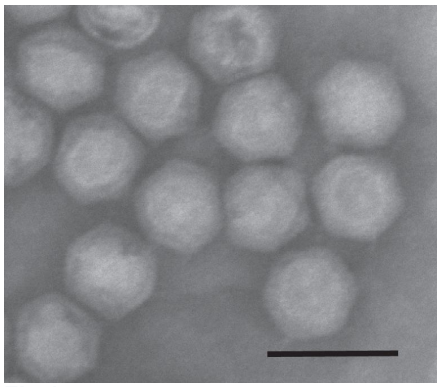

Fig 1

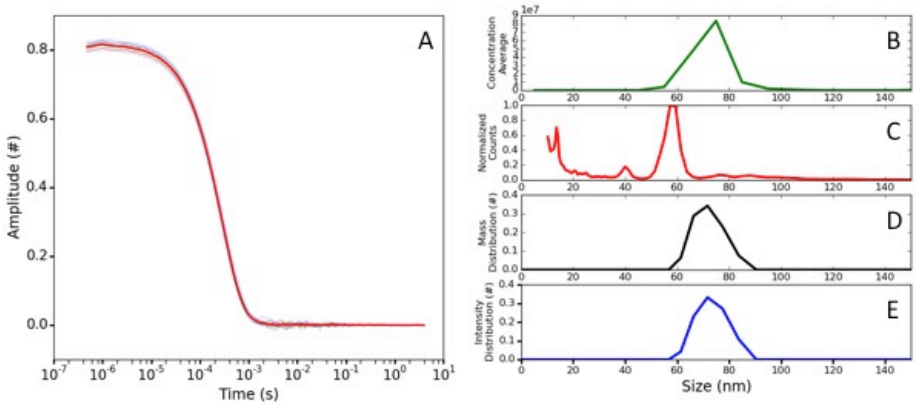
A
B
C
D
E
Amplitude (#)
Time (s)
Size (nm)

Fig 2

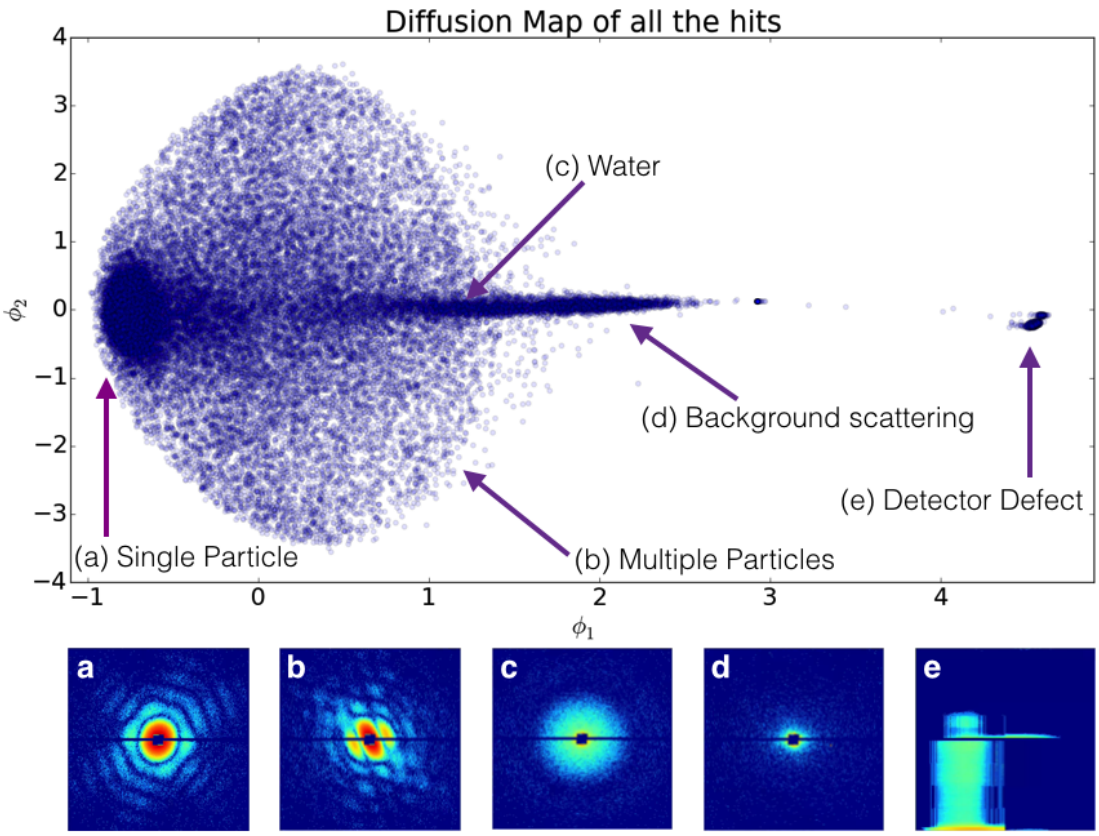
Diffusion Map of all the hits
(c) Water
(d) Background scattering
(e) Detector Defect
(a) Single Particle
(b) Multiple Particles
ϕ_1
ϕ_2
a
b
c
d
e

Fig 3

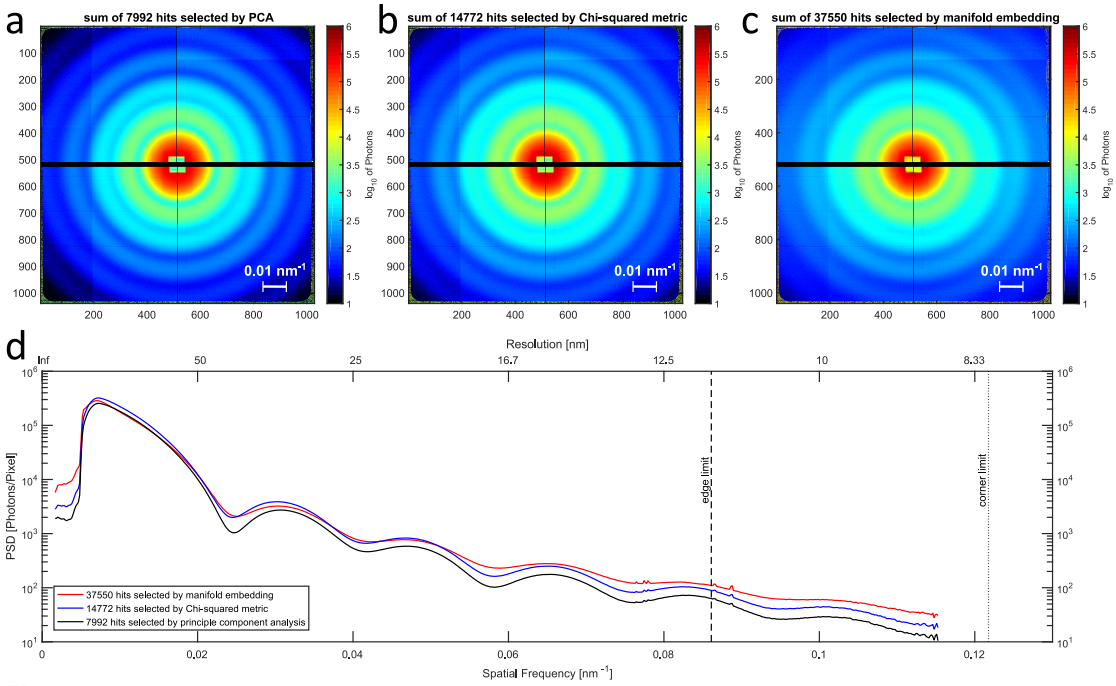

Fig 4

Figure Legends

Fig 1: Electron micrograph of purified bacteriophage PR772. Scale bar represents 100 nm.

Fig 2: NTA measurements (B) of bacteriophage PR772 in ammonium acetate buffer (250mM, pH 7.5). The curve shows the distribution of the different sized particles in the solution. We observed a single large peak at 75 nm with concentration of 10^8 particles/mL, which is similar to the dilution used for measurement. The diameter peak from the DMA measurement (C) was approximately 60 nm. The actual gas flow during the DMA measurement was lower than the set value, which resulted in a diameter low by about 10%. The gas flow was disregarded since the purpose of the DMA measurement was to assess sample purity and not size. DLS measurements of bacteriophage PR772 in ammonium acetate buffer (250mM, pH 7.5). Curve in red shows the average of 18 correlation data collected over time for the sample (A). Curves in black and blue show the size of the particles based on mass (D) and

intensity (E) distribution respectively. The mean diameter of the particle was 75.99 nm with a polydispersity index (PDI) of 0.012.

Fig 3: Diffusion map analysis of all the hits reduced to two dominant dimensions Φ_1 and Φ_2 as described in the text. Clustering helps identify the single particle diffraction patterns in the dataset.

Fig 4: Comparison of single hit selections by principal component analysis (PCA), Chi-sqaured metric and manifold embedding. Summed diffraction patterns of (a) PCA, (b) Chi-squared metric and (c) manifold embedding. (d) Averaged signal over angle (power spectral density, PSD) as a function of spatial frequency and resolution. Five diffraction maxima are fully captured within the detector edges. The sixth maximum is captured within the detector corners.

Tables

References

1. Mazzocco, A., Waddell, T. E., Lingohr, E. & Johnson, R. P. Enumeration of bacteriophages using the small drop plaque assay system. *Methods in molecular biology (Clifton, N.J.)* **501,** 81–5 (2009).
2. Richard Neutze, Remco Wouts, David van der Spoel, Edgar Weckert & Janos Hajdu “Potential for biomolecular imaging with femtosecond X-ray pulses” *Nature* **406**, 752-757 (17 August 2000)
3. Ken R. Ferguson, Maximilian Bucher, John D. Bozek, Sebastian Carron, Jean-Charles Castagn, Ryan Coffee, G. Ivan Curiel, Michael Holmes, Jacek Krzywinski, Marc Messerschmidt, Michael Minitti, Ankush Mitra, Stefan Moeller, Peter Noonan, Timur Osipov, Sebastian Schorb, Michele Swiggers, Alexander Wallace, Jing Yina & Christoph Bostedt “The Atomic, Molecular and Optical Science instrument at the Linac Coherent Light Source” *J. Synchrotron Rad.* **22**, 492–497 (2015)
4. P. Emma, R. Akre, J. Arthur, R. Bionta, C. Bostedt, J. Bozek, A. Brachmann, P. Bucksbaum, R. Coffee, F.-J. Decker, Y. Ding, D. Dowell, S. Edstrom, A. Fisher, J. Frisch, S. Gilevich, J. Hastings, G. Hays, Ph. Hering, Z. Huang, R. Iverson, H. Loos, M. Messerschmidt, A. Miahnahri, S. Moeller, H.-D. Nuhn, G. Pile, D. Ratner, J. Rzepiela, D. Schultz, T. Smith, P. Stefan, H. Tompkins, J. Turner, J. Welch, W. White, J. Wu, G. Yocky & J. Galayda, “First lasing and operation of an ångstrom-wavelength free-electron laser” *Nature Photonics* **4**, 641 - 647 (2010)
5. W. E. White, A. Robert and M. Dunne, “The Linac Coherent Light Source” *J. Synchrotron Rad*. **22**, 472-476 (2015)
6. A. Aquila, A. Barty, C. Bostedt, S. Boutet, G. Carini, D. dePonte, P. Drell, S. Doniach, K. H. Downing, T. Earnest, H. Elmlund, V. Elser, M. Gühr, J. Hajdu,

J. Hastings, S. P. Hau-Riege, Z. Huang, E. E. Lattman, F. R. N. C. Maia, S. Marchesini, A. Ourmazd, C. Pellegrini, R. Santra, I. Schlichting, C. Schroer, J. C. H. Spence, I. A. Vartanyants, S. Wakatsuki, W. I. Weis & G. J. Williams "The linac coherent light source single particle imaging road map" *Struct. Dyn.* **2**, 041701 (2015)

7. Max F. Hantke, Dirk Hasse, Filipe R. N. C. Maia, Tomas Ekeberg, Katja John, Martin Svenda, N. Duane Loh, Andrew V. Martin, Nicusor Timneanu, Daniel S. D. Larsson, Gijs van der Schot, Gunilla H. Carlsson, Margareta Ingelman, Jakob Andreasson, Daniel Westphal, Mengning Liang, Francesco Stellato, Daniel P. DePonte, Robert Hartmann, Nils Kimmel, Richard A. Kirian, M. Marvin Seibert, Kerstin Mühlig, Sebastian Schorb, Ken Ferguson, Christoph Bostedt, Sebastian Carron, John D. Bozek, Daniel Rolles, Artem Rudenko, Sascha Epp, Henry N. Chapman, Anton Barty, Janos Hajdu & Inger Andersson "High-throughput imaging of heterogeneous cell organelles with an X-ray laser" *Nature Photonics* **8**, 943–949 (2014)
8. Anna Munke, Jakob Andreasson, Andrew Aquila, Salah Awel, Kartik Ayyer, Anton Barty, Richard J. Bean, Peter Berntsen, Johan Bielecki, Sébastien Boutet, Maximilian Bucher, Henry N. Chapman, Benedikt J. Daurer, Hasan DeMirci, Veit Elser, Petra Fromme, Janos Hajdu, Max F. Hantke, Akifumi Higashiura, Brenda G. Hogue, Ahmad Hosseinizadeh, Yoonhee Kim, Richard A. Kirian, Hemanth K.N. Reddy, Ti-Yen Lan, Daniel S.D. Larsson, Haiguang Liu, N. Duane Loh, Filipe R.N.C. Maia, Adrian P. Mancuso, Kerstin Mühlig, Atsushi Nakagawa, Daewoong Nam, Garrett Nelson, Carl Nettelblad, Kenta Okamoto, Abbas Ourmazd, Max Rose, Gijs van der Schot, Peter Schwander, M. Marvin Seibert, Jonas A. Sellberg, Raymond G. Sierra, Changyong Song, Martin Svenda, Nicusor Timneanu, Ivan A. Vartanyants, Daniel Westphal, Max O. Wiedorn, Garth J. Williams, Paulraj Lourdu Xavier, Chun Hong Yoon & James Zook "Coherent diffraction of single Rice Dwarf virus particles using hard X-rays at the Linac Coherent Light Source" *Scientific Data* **3**, 160064 (2016)
9. D P DePonte, U Weierstall, K Schmidt, J Warner, D Starodub, J C H Spence & R B Doak "Gas dynamic virtual nozzle for generation of microscopic droplet streams" *J. Phys. D: Appl. Phys.* **41** 195505
10. M. Marvin Seibert, Tomas Ekeberg, Filipe R. N. C. Maia, Martin Svenda, Jakob Andreasson, Olof Jönsson, Duško Odić, Bianca Iwan, Andrea Rocker, Daniel Westphal, Max Hantke, Daniel P. DePonte, Anton Barty, Joachim Schulz, Lars Gumprecht, Nicola Coppola, Andrew Aquila, Mengning Liang, Thomas A. White, Andrew Martin, Carl Caleman, Stephan Stern, Chantal Abergel, Virginie Seltzer, Jean-Michel Claverie, Christoph Bostedt, John D. Bozek, Sébastien Boutet, A. Alan Miahnahri, Marc Messerschmidt, Jacek Krzywinski, Garth Williams, Keith O. Hodgson, Michael J. Bogan, Christina Y. Hampton, Raymond G. Sierra, Dmitri Starodub, Inger Andersson, Saša Bajt, Miriam Barthelmess, John C. H. Spence, Petra Fromme, Uwe Weierstall, Richard Kirian, Mark Hunter, R. Bruce Doak, Stefano Marchesini, Stefan P. Hau-Riege, Matthias Frank, Robert L. Shoeman, Lukas Lomb, Sascha W. Epp, Robert Hartmann, Daniel Rolles, Artem Rudenko, Carlo Schmidt, Lutz Foucar, Nils Kimmel, Peter Holl, Benedikt Rudek, Benjamin Erk, André Hömke, Christian Reich, Daniel Pietschner, Georg Weidenspointner, Lothar Strüder, Günter Hauser, Hubert Gorke, Joachim Ullrich, Ilme Schlichting, Sven Herrmann, Gerhard Schaller, Florian Schopper, Heike Soltau, Kai-Uwe Kühnel, Robert Andritschke, Claus-Dieter Schröter, Faton Krasniqi, Mario Bott, Sebastian Schorb, Daniela Rupp, Marcus Adolph, Tais Gorkhover, Helmut Hirsemann, Guillaume Potdevin, Heinz Graafsma, Björn Nilsson,

Henry N. Chapman & Janos Hajdu “Single mimivirus particles intercepted and imaged with an X-ray laser” *Nature* **470**, 78–81 (03 February 2011)
11. Lothar Strüder,Sascha Epp, Daniel Rolles, Robert Hartmann, Peter Holl, Gerhard Lutz, Heike Soltau, Rouven Eckart, Christian Reich, Klaus Heinzinger, Christian Thamm, Artem Rudenko, Faton Krasniqi, Kai-Uwe Kühnel, Christian Bauer, Claus-Dieter Schröter, Robert Moshammer, Simone Techert, Danilo Miessner, Matteo Porro, Olaf Hälker, Norbert Meidinger, Nils Kimmelc, Robert Andritschke, Florian Schopperc, “Large-format, high-speed, X-ray pnCCDs combined with electron and ion imaging spectrometers in a multipurpose chamber for experiments at 4th generation light sources” Nuclear Instruments and Methods in Physics Research Section A. **614**, 483-496 (2010)
12. Tomas Ekeberg, Martin Svenda, Chantal Abergel, Filipe R. N. C. Maia, Virginie Seltzer, Jean-Michel Claverie, Max Hantke, Olof Jönsson, Carl Nettelblad, Gijs van der Schot, Mengning Liang, Daniel P. DePonte, Anton Barty, M. Marvin Seibert, Bianca Iwan, Inger Andersson, N. Duane Loh, Andrew V. Martin, Henry Chapman, Christoph Bostedt, John D. Bozek, Ken R. Ferguson, Jacek Krzywinski, Sascha W. Epp, Daniel Rolles, Artem Rudenko, Robert Hartmann, Nils Kimmel, & Janos Hajdu “Three-Dimensional Reconstruction of the Giant Mimivirus Particle with an X-Ray Free-Electron Laser” *Phys. Rev. Lett.* **114**, 098102 (2015)
13. Benedikt J. Daurer, Max F. Hantke, Carl Nettelblad, & Filipe R. N. C. Maia “Hummingbird: monitoring and analyzing flash X-ray imaging experiments in real time” *J. Appl. Cryst.* **49**, 1042–1047 (2016)
14. D. Damiani, M. Dubrovin, I. Gaponenko, W. Kroeger, T. J. Lane, A. Mitra, C. P. O'Grady, A. Salnikov, A. Sanchez-Gonzalez, D. Schneider & C. H. Yoon “Linac Coherent Light Source data analysis using psana” *J. Appl. Cryst.* **49**, 672-679 (2016).
15. Chunhong Yoon “Novel algorithms in coherent diffraction imaging using x-ray free-electron lasers” *Proc. SPIE* **8500**, Image Reconstruction from Incomplete Data VII, 85000H (2012)
16. Filipe R N C Maia “The Coherent X-ray Imaging Data Bank” *Nature Methods* **9**, 854–855 (2012)
17. N. D. Loh “Effects of extraneous noise in Cryptotomography”. *Proc. SPIE* **8500**, Image Reconstruction from Incomplete Data VII, 85000K (2012)
18. A. Hosseinizadeh, A. Dashti, P. Schwander, R. Fung, A. Ourmazd, Structural Dynamics, **2,** 041601 (2015)
19. Bobkov, S. A. et al., Sorting algorithms for single-particle imaging experiments at X-ray free-electron lasers J Synchrotron Rad, International Union of Crystallography (IUCr) **22**, 1345 (2015)

Data Citations